An Autonomous Driving Model Integrated with BEV-V2X

Perception, Fusion Prediction of Motion and Occupancy, and

Driving Planning, in Complex Traffic Intersections

Fukang Li, Wenlin Ou, Kunpeng Gao, Yuwen Pang, Yifei Li, Henry Fan

Ford Motor China Co., ltd, Shanghai, 200082, China

Abstract

The comprehensiveness of vehicle-to-everything (V2X) recognition enriches and holistically

shapes the global Birds-Eye-View (BEV) perception, incorporating rich semantics and integrating

driving scene information, thereby serving features of vehicle state prediction, decision-making

and driving planning. Utilizing V2X message sets to form BEV map proves to be an effective

perception method for connected and automated vehicles (CAVs). Specifically, Map Msg. (MAP),

Signal Phase And Timing (SPAT) and Roadside Information (RSI) contributes to the achievement

of road connectivity, synchronized traffic signal navigation and obstacle warning. Moreover,

harnessing time-sequential Basic Safety Msg. (BSM) data from multiple vehicles allows for the

real-time perception and future state prediction. Therefore, this paper develops a comprehensive

autonomous driving model that relies on BEV-V2X perception, Interacting Multiple model

Unscented Kalman Filter (IMM-UKF)-based fusion prediction, and deep reinforcement learning

(DRL)-based decision making and planning. We integrated them into a DRL environment to

develop an optimal set of unified driving behaviors that encompass obstacle avoidance, lane

changes, overtaking, turning maneuver, and synchronized traffic signal navigation. Consequently,

a complex traffic intersection scenario was simulated, and the well-trained model was applied for

driving planning. The observed driving behavior closely resembled that of an experienced driver,

exhibiting anticipatory actions and revealing notable operational highlights of driving policy.

Keywords

Autonomous Driving; Connected and Automated Vehicles; BEV-V2X; Motion and Occupancy

Prediction; Decision-Making; Driving Planning and Control.

I. INTRODUCTION

Cooperative Intelligent Transport Systems (C-ITS) based on vehicle-to-everything (V2X) communication has considerably developed in recent years, bringing us closer to utilizing V2X for autonomous driving and assistance guidance [1], [2]. Due to the numerous substantial benefits provided by C-ITS, governmental authorities worldwide have initiated the allocation of dedicated spectrum for V2X technologies, on a license-exempt basis in the 5.9 GHz band for the cellular based Cellular-V2X (C-V2X) PC5 technology [3], [4].

The characteristics of 5G technologies including enhanced Mobile Broadband (eMBB) and massive Machine Type Communications (mMTC) are pivotal in vehicular communications [5], [6]. Furthermore, facilitating Ultra-Reliable and Low-Latency Communications (URLLC) of 5G is a fundamental element of advanced V2X applications [7], [8]. The application communication of PC5 in vehicle-to-vehicle (V2V) or infrastructure-to vehicle (V2I), as shown in Fig. 1, results in quicker connections, reduced latency, enhanced reliability, increased capacity, and broader coverage [9]–[11], significantly reducing issues caused by temporal asynchrony [12]. The temporal asynchrony challenges in V2X have seen an emergence of numerous solutions, addressing the more intricate aspects. Z. Lei et al. [13] developed SyncNet to align V2V collaboration messages through latency-aware attention. [14] introduced CoBEVFLow to address irregular asynchrony issue. Furthermore, the fusion misalignment arising from temporal, spatial asynchrony and limited wireless communication has been remarkably mitigated by Feature Flow Net (FFNet) [15]. These contribute to real-time matching of road connectivity, road events, traffic signals, and information from other connected vehicles with CAVs through V2X communication.

Additionally, the fusion of perception and prediction in the V2I and V2V domains incorporating CAVs and roadside multi-sensor architectures has attracted much interest among researchers in the ITS-V2X field [16]–[18]. Infrastructure sensors, such as cameras and LiDARs, are often placed considerably higher than ego vehicles for a wider field of view. The utilization of additional data from these infrastructure sensors can significantly enhance the acquisition of valuable information and enhance the perceptual capabilities of autonomous driving systems [19]. Many fusion frameworks for the data integration between CAVs and infrastructure devices has been proposed for cooperative perception, forming comprehensive, precise, simultaneous fusion and prediction models for ITS-V2X [15], [20]–[22]. These advancements paves the way for the

more precise and real-time enrichment of V2X communication message sets, including Map Msg. (MAP), Signal Phase And Timing (SPAT) data, Roadside Information (RSI), Basic Safety Msg. (BSM) from the standard (T/CSAE 53-2020) [23].

The V2X message sets enables the comprehensive perception of autonomous driving. Specifically, MAP enables the construction of maps for crossroad areas and establishes upstream and downstream road connectivity. SPAT information is harnessed to establish comprehensive insights into traffic signals based on signal phase and countdown, enabling synchronized traffic signal navigation. RSI data is utilized to describe impact zones associated with road events and traffic signs, offering obstacle positions and range information for the ego vehicle. Additionally, the utilization of time-stamped BSM data from multiple vehicles assists in determining current vehicle positions, speeds, heading angles, and predicting future vehicle states. The V2X data [23] provides a reliable and rich foundation for the subsequent prediction, decision-making, planning, and control in autonomous driving.

However, deploying untested algorithms directly onto a real autonomous-driving platform for road testing is known to be costly, time-consuming, and dangerous. Hence, it is crucial to perform extensive and dependable offline tests before deploying algorithms on an actual autonomous driving vehicle [24]–[26]. The validation and testing of cooperative driving relies heavily on the use of simulation environments. Hardware-In-the-Loop (HIL) simulation systems offer a cost-effective and efficient means of rapidly testing autonomous driving algorithms and hardware across a diverse range of virtual scenarios. Simulation experiments employing the HIL system serve to validate the effectiveness of autonomous driving algorithms in virtual environments, encompassing aspects like perception, planning, decision-making, and control [27].

The proposed HIL simulation system is composed of both infrastructure and ego CAV sides, which jointly form an integrated system for testing and verification in a closed-loop method.

The infrastructure side mainly includes three parts:

- 1) The virtual environment constructing software part, which simulates real traffic scenarios.
- 2) The V2X message sets generating software part, fusing perception and producing comprehensive V2X message sets.
- 3) The Road Side Unit (RSU) hardware part, broadcasting and receiving V2X message sets using PC5 communication.

The ego CAV side also primarily contains three sections:

- 1) The In-Car System section including Telematics Control Unit (TCU) and In-Vehicle Infotainment (IVI), which analyzes and processes the V2X message sets and display the location of real-time ego vehicle.
- 2) The controller model section, utilizing perception data, processing it into a BEV view and advanced data, and applying an deep reinforcement learning environment to perform motion and occupancy prediction, decision-making, and driving planning.
- 3) The On Board Unit (OBU) hardware part, receiving and sending V2X message sets using PC5 communication.

As shown in Fig.1, the whole figure demonstrates the HIL simulation process. The blue rectangle in the figure illustrates the simulated infrastructure side and the red rectangle exhibits the simulated ego CAV side.

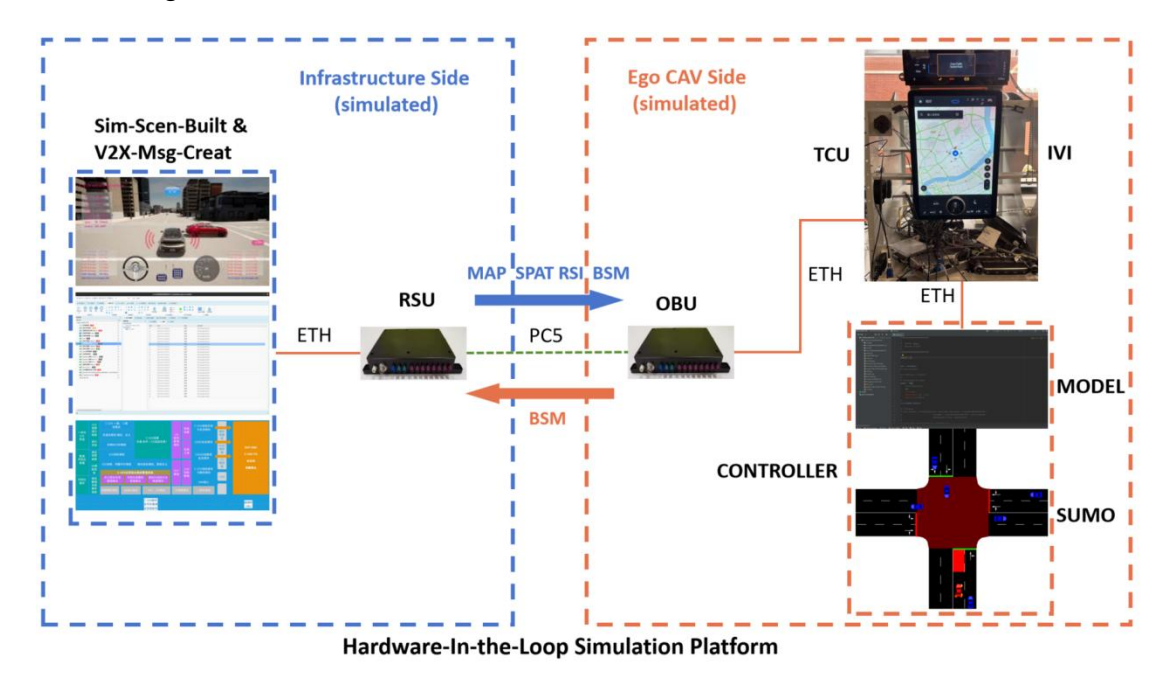


Fig. 1 the whole Hardware-In-the-Loop (HIL) simulation environment

In a simulation software stack that operates both on offline computers and in-vehicle systems, it encompasses interconnected components for simulating traffic scenarios, receiving V2X message sets and broadcasting between roadside and in-vehicle units, as well as conducting ego vehicle driving planning and control. The software layer simulates perception data and vehicle states, forwarding them to core algorithms.

II. RELATED WORKS

A. BEV-V2X Perception

The objective of the perception module is to generate an intermediate-level representation of the environmental states (e.g., a bird's-eye view map displaying all obstacles and agents) that is to be subsequently employed by the decision-making system to formulate the driving policy. This representation encompasses lane positioning, drivable areas, the positions of other agents such as vehicles and pedestrians, as well as the status of traffic lights and other relevant factors. [28].

Bird-Eye-View (BEV) effectively presents the position and range of scenario elements in a concise and semantic way, relying on an occupancy grid as a foundation [29]. Typically, BEV is depicted as an image with a specific resolution, where each pixel corresponds to a predefined grid unit dimension [30]. BEV data include abundant semantic content, capable of amalgamating environmental details, road characteristics, and both the stationary and moving attributes of traffic participants [29]. A single BEV frame captures the driving state and relationships of all traffic participants at a specific timestamp in a particular road scenario, while a continuous sequence of BEV frames represents the driving behavior and interactions of these participants over a defined spatial and temporal range [31]. BEV data is of significance when it comes to creating a unified scenario representation across research areas like motion and occupancy prediction [32], [33], driving planning [34], [35], and control [36], [37].

However, establishing a real-time, precise, and globally semantic BEV has always been a challenge in the field of recognition. With the backing of PC5, allowing for quicker connections, reduced latency, and enhanced reliability, V2X communication significantly contributes to the realization of global BEV perception. This is made possible through the mature acquisition system with infrastructure sensors and the capacity for data fusion between infrastructure and vehicles [17]. There are essentially two primary communication modes for achieving BEV integration through Vehicle-to-Vehicle (V2V) and Vehicle-to-Infrastructure (V2I) communication in the context of V2X technology. Therefore, at the current stage, a substantial academic effort is concentrated on how to utilize V2X to efficiently and accurately integrate perception information from roadside infrastructure and Connected and Autonomous Vehicles (CAVs), rapidly consolidating it into a global BEV data for comprehensive environmental cognition around the vehicle. R Xu et al. [21] developed V2X-ViT model within a cohesive Transformer framework

capable of addressing common challenges in V2X applications, including asynchronous information exchange, pose inaccuracies, and the diversity of V2X components. V2XFormer, as proposed by T Wang *et al.* [38], consists of extraction and alignment of multi-local BEV information and V2X fusion through V2X communication, outperforming the single-vehicle model in both perception and prediction tasks. Chang *et al.* [22] introduced a cooperative BEV fusion and prediction model called BEV-V2X to fuse and forecast the forthcoming global BEV occupancy grid map using the local BEV data collected from roadside unit or cloud center and data from all CAVs within a defined control area. Notably, BEV-V2X demonstrates a robust capability to accurately estimate and predict global spatial-temporal changes, even in scenarios where not all vehicles are CAVs.

Meanwhile, an increasing number of V2X-based BEV perception databases are being established to facilitate the availability of training and validation data for various scenarios and functionalities. Y Li et al. [39] created the V2X-Sim dataset by simulation, offering synchronized BEV recordings from both roadside infrastructure and multiple vehicles at intersections, fostering collaborative perception capabilities. T Wang et al. [38] used CARLA realistic simulator to build the DeepAccident, a comprehensive dataset encompassing a wide range of accident scenarios commonly encountered in real-world driving. H Yu et al. [16] introduced the DAIR-V2X dataset, derived from real scenarios. This multi-modal and multi-view dataset includes LiDAR and camera frames captured in real-world scenes, providing support for Vehicle-Infrastructure Cooperative Autonomous Driving (VICAD). All of these BEV-V2X fusion methods and associated datasets pave the path towards enhancing message sets (comprising MAP, SPAT, RSI, BSM) in V2X communication with greater precision and real-time updates.

B. Motion and Occupancy Prediction

Motion and occupancy prediction is pivotal for CAVs to improve the safety by predicting the future conditions and states of ambient environment and other traffic participants. In particular, representing the predicted movements of traffic participants through future motion trajectories can offer instructive information for decision-making and driving planning [40]–[42]. Accurate prediction of future occupancy enables proactive identification of potential hazards, warning of vehicle collisions, and becomes an indispensable factor in enhancing the safety of autonomous driving systems [43].

Motion prediction challenges involve utilizing the historical states of traffic participants to estimate their forthcoming states. The states of traffic vehicles at the future times should be presented, commonly including the location, velocity and orientation of vehicles [41]. Occupancy grid map is a discretized BEV representation containing occupied elements. The task of occupancy prediction involves anticipating how the grid map will evolve in the future to effectively represent objects and collision boundaries [44], [45]. Recently, the fusion prediction methods based on the Bayesian probability theory, such as the Kalman filter, have garnered significant attention due to their consideration of uncertainty and noise.

The future states of vehicle predicted is typically considered as imperfectly determined, subjected to inherent noise and interference derived from observational data [46], [47]. Barrios, C et al. [48] introduced the KF to address inaccuracies associated with various potential states of a vehicle. By iteratively combining the prediction and update steps in a recursive loop, the mean value and covariance matrix for the vehicle's states can be relatively determined at multiple future time steps [49]. This process allows us to calculate a trajectory that is averaged while taking into account the related uncertainties [50]. Nevertheless, the tracking precision of KF method may fall behind when confronted with non-linear scenarios, particularly in cases where the vehicle's velocity or acceleration undergo continuous variations [51]. On this basis, several scholars have recommended filtering methods better designed to address nonlinear systems. Jiang et al. [52] introduced the Extended Kalman Filter (EKF) approach for the estimation of the lateral state of an automobile, encompassing parameters such as speed, slip angle, acceleration. Alexander K [53] introduced an adaptive fuzzy EKF, a state estimation technique to predict the vehicle's dynamic characteristics. These above methods are capable of determining the vehicle's motion and occupancy state through the utilization of vehicle kinematic principles, a fundamental requirement for most advanced intelligent vehicle control systems.

Furthermore, the application of higher-order filters [54], such as second-order filters, is employed to address the challenges posed by frequent speed or acceleration variations in real-world driving scenarios. The Unscented Kalman Filter (UKF), [55] as a method that approximates a Gaussian distribution rather than approximating a nonlinear function, has gained increasing attention due to its ability to maintain second-order accuracy while keeping computational costs low. The UKF algorithm offers improved practicality when compared to the

EKF, as it avoids the potential truncation errors associated with Taylor expansion and obviates the requirement for solving the Jacobian matrix [54]. H Wu *et al.* [56] utilized the UKF approach to attain precise motion estimation and prediction, resulting in a root mean square error (RMSE) of just 0.1 m in robot positioning. H Gao *et al.* [57] used the UKF filter to achieve high precision for vehicle maneuver trajectory prediction. These findings consistently demonstrate that UKF offers superior accuracy in the prediction of future vehicle states.

Moreover, motion and occupancy prediction of vehicles is inherently non-deterministic due to its dependence on various scenarios and their unpredictability [58], such as road curvature, phase and countdown of traffic lights, and complex connectivity in junctions. Therefore, vehicle states prediction is addressed using a range of motion models in several research strategies [59], [60]. W. Blair [61] develops an innovative vehicle position prediction algorithm rooted in the constant velocity (CV) model. Zhang *et al.* [62] utilize constant acceleration (CA) model to develop kinematic positioning approach. M. Deng *et al.* [63] proposed current statistical (CS) model and cubature Kalman filter method to accurately predict the turning maneuver trajectory of the ego vehicle.

Nevertheless, when dealing with variable motion patterns, the predictive accuracy of a single motion model tends to degrade. Hence, utilizing Interacting Multiple model (IMM) to assist real-time or predictive switching of motion models is a crucial endeavor for precise prediction. H Gao et al. [57] proposed a IMM-UKF algorithm to achieve motion and occupancy prediction with high accuracy for intelligent vehicles. Their IMM model combines the vehicle dynamics model, vehicle kinematics model, and maneuver recognition-based model using the UKF filter to achieve high precision. MT Abbas et al. [64] used the EKF with the integration of IMM, combined with constant velocity (CV) model, constant acceleration (CA) model, vehicle turn (VT) model and other models, estimating the vehicle future occupancy and kinematic states. Once a comprehensive range of potential scenarios and motion models for a vehicle has been established, probability density functions (PDFs) are subsequently computed. Among these PDFs, the model with the highest likelihood is chosen for predicting the future position of the vehicle. This entire process is executed by means of the IMM algorithm, which integrates the probabilities associated with each model through the utilization of a Markov model [65]. Ultimately, a final transition metric is formulated, taking into account all the probabilities.

C. Decision-Making, Driving Planing and Control

By incorporating perceptions of all environmental states (including drivable areas, the positions of all vehicles and pedestrians, and the status of traffic lights), coupled with predictions of future motion and occupancy for traffic participants, one can attempt to guide agents to model the uncertain interaction with environment and other traffic participants using decision-making and planning methods [66]. This approach forms the basis for driving strategies that prioritize safety and predictability within complex and cluttered traffic environments, such as intersections.

The agent faces the challenge of making real-time predictive decisions while navigating, incorporating newly acquired environmental information from its surroundings. This challenge is amplified by a high dimensinal space given the number of unique configurations, such as traffic rules, safety and comfort, through which the agent and environment interact, resulting in a complex and combinatorially large problem. In these scenarios, our objective is to address a sequential decision-making process and make optimal decisions in real-time. In this context, optimal planning and control can be seen as a model-based Reinforcement Learning (RL) problem, where the dynamics of the vehicle and its interaction with the environment are characterized by well-defined differential equations. RL methods have been developed to address stochastic decision-making and planning problems as well as ill-posed challenges that involve unknown rewards and state transition probabilities [28].

RL methods facilitate model learning by allowing it to acquire task proficiency through a process of trial and error. This learning paradigm can be formally represented as a Markov decision process, formally described as a tuple (S, A, P, R), where S signifies the state space, A represents the action space of possible actions, P denotes the state transition probability model, and R characterizes the reward function. At each discrete time-step the agent observes a set of states S_t , takes an action a_t from the set of possible actions A, and subsequently, the environment undergoes a transition based on P. The agent then observes a new set of states S_{t+1} and receives a reward r_t . The goal of the agent is to learn a policy $\pi(S_t, a_t)$, which maps observations to actions in a way that maximizes the cumulative rewards. Consequently, the agent learns from its own actions during interactions with the environment and obtains an evaluation of its performance through the reward function [67].

Value-based algorithm is a category of RL algorithms, such as Q-learning [68], which focuses on estimating the value function V(s), representing the value (expected reward) associated with a specific state. When the state transition dynamics P are known, the policy can choose actions that lead to states where expected rewards are maximized. However, in many RL scenarios, the environment model is unknown. In such cases, the state-action value or quality function Q(s, a) is utilized instead. This function estimates the value of a particular action in a given state. The optimal policy is then determined by maximizing the state-action value function Q(s, a) in a greedy way.

In real-world scenarios, handling continuous state and action spaces often involves discretization. However, excessive discretization can limit performance, and fine-grained discretization may result in a large state-action space, making sample collection impractical. Alternatively, function approximation methods, especially deep neural networks, are used in Deep Reinforcement Learning (DRL) to generalize across states and actions, addressing complexities and extending knowledge to new state-action pairs. Deep Q-Networks (DQN) [69], a deep reinforcement learning algorithm, combines a variant of Q-learning algorithm with deep neural networks (DNNs). DNNs serve as a non-linear function approximator for state spaces of high dimension. The O(s, a) function is represented by a DNN that forecasts the value of all available actions based on the input state. Therefore, the process of determining the most suitable action involves executing a forward pass through the network to form experience trajectories. In additional, to enhance efficiency in utilizing samples, the agent's experiences are preserved within a replay memory (experience replay). Q-learning updates are then applied to samples chosen at random from this replay memory to update the network. For better robustness, DQN employs two networks where the parameters of the target network remain fixed for a set number of iterations before updates are made to the online network's parameters.

M Zhou et.al [70] proposed a DRL car following model based on Deep Deterministic Policy Gradient (DDPG), a combination of DQN and DPG. Their trained central controller can utilize the advantage of CAVs communicating with surrounding vehicles and traffic light systems to enhance travel efficiency, safety, and to reduce fuel consumption for CAVs when crossing signalized intersections. In order to reduce the computation time and realize collision-free driving, Y Guan et.al [71] developed a DRL algorithm called generalized exterior point to find a neural network

solution offline. These authors [72], [73] utilized Proximal Policy Optimization algorithm (PPO) to execute high-level decisions, trajectory and driving commands to infer ego vehicle-desired behavior in signalized and non-signalized traffic intersection.

D Isele et.al [74] conducted a comparative analysis between the Time-to-Collision (TTC) algorithm and the DQN algorithm, evaluating their capacity to acquire exploratory behaviors for navigating occluded intersections. Their findings indicate that DQN approaches demonstrate sound policies, successfully achieving the goal in 98.46% of instances within challenging scenarios, considerably outperforming other methods. G Li et.al [75] utilized the DQN algorithm to derive the optimal driving policy focused on both safety and efficiency. To verify the effectiveness of their decision-making framework, they simulated the top three intersection scenarios with a high risk of accidents involving crossing intersections. The results show that the method they developed could guide AVs to navigate intersections safely and efficiently in all the tested scenarios. The similar experiments and results can be seen in [76]. Some researchers [77] also proposed a risk-aware DQN approach for decision making, incorporating a risk-based reward function which punishes risky situations instead of only collision failures, learning more reliable policies which are safer in challenging situations. T Tram et.al [78] employed DRON [79] method, which combined a Long Short Term Memory (LSTM) with a DQN, for decision-making, planning and control purposes. This method was designed for automated vehicles that negotiate with other possibly non-automated vehicles in intersections, resulting in a significant lower collision to timeout ratio than previous algorithm.

III. AN AUTONOMOUS DRIVING MODEL

A. BEV-V2X Perception

This section utilizes the V2X message sets to generate the BEV map and more detailed perception information. Customizing the generation of perception information for various functionalities involves using specific content within different message sets, and transforming the latitude and longitude information into local coordinate content. Firstly, for the road connectivity functionality, global drivable area information is generated using MAP data. Secondly, for other vehicles information, real-time vehicle occupancy and states are generated using BSM data. Regarding traffic signal light information, the MAP and SPAT are collaborated to generate signal information for the road where the ego vehicle is located. For road event and traffic sign

information, dangerous area position and ranges are generated using RTE and RTS from the RSI, respectively. The detailed structure and explanations are provided in the following contents.

Road Connectivity:

Map

nodes: a list of intersections information

id: the Id of this intersection (1) refPos: 3D position of the center of this intersection, including: latitude, longitude, elevation, inLinks: a collection of directed roads connecting to this intersection (2) **laneWidth**: the width of a single lane or a single inLink (3) **name**: description about the relationship between nodes of this inLink points: a list of midpoint vector points for current inLink **posOffset**: relative position deviation between refPos and points offsetLL: the latitude and longitude deviation (4) offsetV: the elevation deviation lanes: a list of lanes information of this road (5) **laneID**: the Id of a single lane points: a list of midpoint vector points for this lane connectsTo: connectivity between current and downstream lane **connectinglane**: the data about downstream lanes lane: the Id of downstream lane (6) maneuver: permitted types of turning

upstreamNodeId: the upstream intersection Id connected to this road

- (1) refPos: (lat, long)
- (2) laneWidth: width
- (3) name: "id1-id2"
- (4) points: [(offset_lat, offset_long), (...) ...]
- (5) inLinks: {{name1, points, laneWidth}, {...}, ...} = {{"id1-id2" [(offset_lat, offset_long), (...) ...], width}, {...}, ...}
- (6) \rightarrow other inLinks: $\{...\}, \{...\}, \{...\}$

Transform to BEV and observation information:

- 1) refPos (lat, long) \rightarrow O (x_o, y_o) as the refPos is the center of the intersection, assume this as the origin O (0,0)
- name "id1-id2" → inLinkName "id1-id2"
 define the name of this inLink, implying from a node id to other node id.
- 3) points $[(offset_lat, offset_long), (...) ...] \rightarrow pointsinLink[(x_l, y_l), (...) ...]$
- 4) inLink { "id1-id2", [($offset_lat, offset_long$), (...) ...], width} \rightarrow inLinkMap {"id1 id2", [(x_1, y_1), (...) ...], width}

describe this inLink, including name, the coordinates of all points and occupied width

5) Other inLinks: {...},{...} →inLinkMap(1){}, inLinkMap(2){}, inLinkMap(3){} depict the contents of all downstream inLinks.

Other vehicles information

BSM

bsmFrame: the information of this traffic participant

id: temporary vehicle Id

secMark: the millisecond-level when this bsm message is transmitted

pos: current 3D position of this traffic participant,

including: elevation, latitude, longitude

speed: the velocity of this traffic participant

heading: the yaw angle of this traffic participant

size: the size of this vehicle, including: width, length, height

(1) bsm [id: *vehicleId*, secMark: *timestamp*, pos(*lat*, *long*), speed: *velocity*, heading: *yaw angle*, size(*width*, *length*)]

Transform to BEV and observation information:

bsm [] → bsm

(1)

[vehicleId, timestamp, ($x^{vehicleId}$, $y^{vehicleId}$), velocity, yaw angle, (width, length)] In the BEV representation, the lateral and longitudinal coordinates ($x^{vehicleId}$, $y^{vehicleId}$) of the vehicle define its center of gravity (considered as the center point in this paper). Subsequently, based on the yaw angle, width, and length of the vehicle, the maximum and minimum values for the occupied lateral and longitudinal coordinates [$x^{vehicleId}_{min}$, $x^{vehicleId}_{max}$, $y^{vehicleId}_{min}$, $y^{vehicleId}_{max}$] are computed. The region encompassing these four extremities is then used to fill the vehicle grid occupancy in the BEV representation

Traffic Signal Light Information:

(3)

Map

nodes: a list of intersections information

id: the Id of this intersection

inLinks: a collection of directed roads connecting to this intersection

lanes: a list of lanes information of the road

(1) laneID: the Id of the current single lane
connectsTo: connectivity between current and downstream lane
phaseId: traffic signal phase Id of this lane

movements: a list of the signal phase Ids associated with this road

- (2) connected here. Particularly, this phase Id is the unique linkage between the MAP message and the SPAT message phaseId: current traffic signal phase Id
- (1) lane: (laneId, phaseId1, phaseId2)
- (2) movements: (phaseId1, phaseId2, phaseId3, ...)
- (3) inLinks: {[lane1, lane2, ...], movements} = {[(laneId1, phaseId1, phaseId2), (...), ...], (phaseId1, ...)}

Transform to BEV and observation information:

- 1) lane (laneId, phaseId1, phaseId2) → lane2phaseId (laneId, phaseId1, phaseId2) describe the relationship between lane and traffic light data (phase and countdown)
- 2) movements (*phaseId1*, *phaseId2*, ...) → phaseIdSet (*phaseId1*, *phaseId2*, ...) define a set including all phaseIds related to this current inLink.
- 3) inLink {[(laneId1, phaseId1, phaseId2), (...), ...], (phaseId1, ...)} → inLinkTL {[(laneId1, phaseId1, phaseId2), (...), ...], (phaseId1, ...)}

depict this current inLink's information of all lanes and traffic light data, and its relationships.

SPAT

intersections: a list of intersections information

intersectionId: the Id of this current intersection mov: UTC time in minutes phases: a list of the information of traffic signal phases id: this current phase id phaseStates: current states of this traffic signal phase **light**: description of this light, including: "v2i green", (4) "v2i yellow", "v2i red". timing: a signal phase status in countdown form (3) **likelyEndTime**: the estimated time remaining (2) from the current to the end of this phase (1) nextDuration: the duration of time that will pass after next start of this phase state startTime: the time remaining until the start of this phase state from current moment timeStamp: milliseconds within a one-minute interval

- (1) timing: (endtime, nextduration, starttime)
- (2) phaseStates:{[light1, timing1], [...], [...]} = {["v2i_green", timing1],["v2i_yellow", timing2],["v2i_red", timing3]}
- (3) phases: {{phaseId1, phaseStates1}, {...}, ...}
- (4) intersection{intersectionId, moy, timeStamp, phases} = {intersectionId, moy, timeStamp, {{phaseId1, phaseStates1}, {...}, ...}}

Transform to BEV and observation information:

- timing: (endtime, nextduration, starttime) →
 countdownTiming: (endtime, nextduration, starttime)
 describe the timing countdown information of the current phase state.
- 2) phaseStates:

```
{["v2i_green", timing1], ["v2i_yellow", timing2], ["v2i_red", timing3]} → phaseStatesTL:
{["v2i_green", countdownTiming1],
["v2i_yellow",countdownTiming2],
```

```
["v2i_red", countdownTiming3]}
```

depict three timing states (green, yellow and red) of one traffic light phase

- 3) phases {{phaseId1, phaseStates1}, {...}, ...}
 - phasesTL {{phaseId1, phaseStatesTL1}, {...}, ...}

illustrate the relationship between phaseId and phaseState

4) intersection {intersectionId, moy, timeStamp, phases} →

intersectionTL {intersectionId, moy, timeStamp, phasesTL}

illustrate all traffic light information of this current intersection, including intersectionId, timestamp and all phases.

Road Event and Traffic Sign Information

RSI

RTS

(5)

(1) refPos: 3D position of the reference position, including: elevation, latitude, longitude rtss: the information of this traffic sign

rtsId: the Id of this rts information

signType: the type of this traffic sign

referencePaths: the associated alert path information for this traffic sign

activePath: a directed coverage area information presented as an ordered list of position points

offsetLL: the latitude and longitude deviation between refPos and this impact point **offsetV**: the elevation deviation between refPos

and this impact point

-pathRadius: the biggest distance away from the alert path within

- which the warning is active
- (1) refPos: (lat, long)
- (2) activePath: [(offset lat, offset long), (...), ...]
- (3) pathRadius: pathradius
- (4) referencePaths: $\{\{\text{activePath1}, pathradius1\}, \{...\}, ...\} = \{\{[(\text{offset lat, offset long}), (...), ...], pathradius1\}, \{...\}, ...\}$
- (5) rtss: {{*rtsId1*, referencePaths1}, {...}, ...}

Transform to BEV and observation information:

1) activePath [(offset_lat, offset_long), (...), ...] \rightarrow activePathPoints [(x^{rtsId} , y^{rtsId}), (...), ...]

describe a list of position points related to the impact area of this traffic sign

2) referencePaths $\{\{\text{activePath1}, pathradius1}, \{...\}, ...\} \rightarrow$

referencePathsArea {{activePathPoints1, pathradius1}, {...}, ...}

depict the associated path information for this traffic sign, including a list of position points and the impact path width (*pathradius*) away from these points.

3) rts: $\{rtsId, referencePaths\} \rightarrow rts: \{rtsId, referencePathsArea\}$

illustrate the information of the traffic sign, including Id,.a list of position points and the impact path area of this traffic sign.

RTE

rtes: a list of the information of road events

rteId: the Id of this rte information

eventType: the type of this road event

eventSource: the event source

eventPos: the relative 3D positional deviation

between refPos and the center of this event

(3)

offsetLL: the latitude and longitude deviation

offsetV: the elevation deviation

(2)

eventRadius: the impact range (radius) of this event

- (1) refPos: (lat, long)
- (2) eventRadius: radius
- (3) eventPos: (offset lat, offset long)
- (4) rtes: {[rteId1, eventPos1, radius1], [...], ...}

Transform to BEV and observation information:

rte: $[rteId, (offset_la1, offset_long), radius] \rightarrow rte: [rteId1, (x^{rteId}, y^{rtId}), radius1]$ describe the information of the road event, including Id, position and the impact radius of this event.

B. Fusion Prediction of Motion and Occupancy

Firstly, for the motion prediction, the vehicle state and control matrices are established, and five different motion models integrated with IMM-UKF approach are applied. This is because creating smaller models tailored to different vehicle scenarios is simpler than setting a single but complex model [64].

Utilizing information obtained from the BSM message set in section II.A, including the positions, velocities, and heading angles of other vehicles, and the data obtained from ego vehicle's sensors, encompassing the position, velocity, acceleration, and heading angle, a unified vehicle state matrix and control parameter matrix are established. The vehicle state matrix, as defined in equation (1), includes the vehicle's position coordinates and velocity components in the x and y directions. The control parameter matrix, defined in equation (2), encompasses the acceleration components in the x and y directions and the relative change in heading angle. The state transition during iterations is described by equation (3).

$$X(t) = [x(t), y(t), v_x(t), v_y(t)]^T$$
(1)

$$U(t) = \left[a_x(t), a_y(t), \Delta\theta(t) \right]^T$$
 (2)

$$X(t+1|t) = X(t|t) + f(X(t|t), U(t))$$
(3)

Five different motion models are established based on distinct behavioral patterns of vehicles. These models include vehicle moving with constant velocity, vehicle moving with constant acceleration, vehicle is static or not moving, vehicle moving with constant jerk, and vehicle turning model. Jerk can be defined as the rate of change of acceleration [64]. The involved vehicle control parameter matrices and state transition models of these five motion models are outlined as follows:

1) Constant Location model (CL)

$$U(t) = [0, 0, 0]^{T}$$

$$f(X(t|t), U(t)) = [0, 0, 0, 0]^{T}$$
(4)

2) Constant Velocity model (CV)

$$U(t) = [0, 0, 0]^{T}$$

$$f(X(t|t), U(t)) = [v_{x}(t) \times \Delta T, v_{y}(t) \times \Delta T, 0, 0]^{T}$$
(5)

3) Constant Acceleration model (CA)

$$U(t) = \left[a_x(t), a_y(t), \Delta\theta(t) \right]^{I}$$

$$f(X(t|t), U(t)) = \begin{pmatrix} v_x(t) \times \Delta T + 1/2 \times a_x(t) \times \Delta T^2 \\ v_y(t) \times \Delta T + 1/2 \times a_y(t) \times \Delta T^2 \\ a_x(t) \times \Delta T \\ a_y(t) \times \Delta T \end{pmatrix}$$
(6)

4) Constant Jerk model (CJ)

$$U(t) = \left[a_{x}(t) + j_{x}(t) \times \Delta T, a_{y}(t) + j_{y}(t) \times \Delta T, \Delta \theta(t) \right]^{T}$$

$$f(X(t|t), U(t)) = \begin{pmatrix} v_{x}(t) \times \Delta T + 1/2 \times a_{x}(t) \times \Delta T^{2} + 1/6 \times j_{x}(t) \times \Delta T^{3} \\ v_{y}(t) \times \Delta T + 1/2 \times a_{y}(t) \times \Delta T^{2} + 1/6 \times j_{y}(t) \times \Delta T^{3} \\ a_{x}(t) \times \Delta T + 1/2 \times j_{x}(t) \times \Delta T^{2} \\ a_{y}(t) \times \Delta T + 1/2 \times j_{y}(t) \times \Delta T^{2} \end{pmatrix}$$
(7)

5) Vehicle Turn model (VT)

$$f(X(t|t), U(t)) = \begin{cases} (v_x(t)\cos(\Delta\theta(t)) + v_y(t)\sin(\Delta\theta(t))) \times \Delta T \\ (v_y(t)\cos(\Delta\theta(t)) - v_x(t)\sin(\Delta\theta(t))) \times \Delta T \\ v_x(t)(\cos(\Delta\theta(t)) - 1) + v_y(t)\sin(\Delta\theta(t)) \\ v_y(t)(\cos(\Delta\theta(t)) - 1) - v_x(t)\sin(\Delta\theta(t)) \end{cases}$$
(8)

Immediate UKF algorithm:

Algorithm 1 Immediate UKF Algorithm

Initialize:

- (1) The initial mean state \hat{x}_0
- (2) The initial covariance P_0

for step episode = 1, Max steps **do**

If $step_episode \neq 1$:

Observation and Validation:

- (1) Calculate the observation vector $\hat{z}(t)$
- (2) Calculate the validation region $\Phi_i(t, \varepsilon^2)$
- (3) Calculate the innovation covariance $P_{zz}(t)$

Update:

- (1) Calculate the near-optimal filter gain K(t) and cross correlation $P_{xz}(t|t-1)$
- (2) Update the estimated mean state $\hat{x}(t|t)$
- (3) Update the error covariance $P_{xx}(t|t)$

Prediction:

- (1) Predict the vehicle state $\hat{x}(t+1|t)$
- (2) Predict the covariance matrix $P_{xx}(t+1|t)$

end

The information recursive update and prediction process must assess diverse uncertainty arising from both process noise and measurement noise. In this article, an Immediate UKF method is specifically designed to effectively manage the impact of noisy information and modeling errors.

Commencing with the representation of the discrete state transition equation of vehicle, considering uncertainty, the following equations are formulated:

$$X(t+1) = F[X(t), q(t), t]$$

$$Z(t) = H[X(t), w(t), t]$$
(9)

where F[X(t)] and q(t) represent the state function and process noise, respectively. And H[X(t)] and w(t) are the observation function and measurement noise, respectively.

1) Initialization: The initialization equations are written as follows:

$$\hat{x}_0 = E[x_0]$$

$$P_0 = E[(x_0 - \hat{x}_0)(x_0 - \hat{x}_0)^T]$$
(10)

where E is the mathematical expectation. Therefore, \hat{x}_0 is the mathematical expectation of x_0 , and P_0 is the variance.

2) Prediction: The state transition equation of vehicle (3) is used to conduct state prediction and observation. The state prediction equation is formulated by instantiating each point to derive a set of transformed sigma points, as follows:

$$X_i(t+1|t) = F[X_i(t), U(t)], \quad i = 0, ..., 2L$$
 (11)

where $F(\cdot)$ represents the state transition function.

The predicted vehicle state (predicated mean state) can be computed using:

$$\hat{x}(t+1|t) = \sum_{i=0}^{i=2L} W_i^m X_i(t+1|t)$$
 (12)

The covariance of the state prediction is calculated according to:

$$P_{xx}(t+1|t) = \sum_{i=0}^{i=2L} W_i^c \{ [X_i(t+1|t) - \hat{x}(t+1|t)] \times [X_i(t+1|t) - \hat{x}(t+1|t)]^T \} + Q(t|t)$$
 where $Q(t|t)$ represents the covariance matrix of the process noise. Every element within the covariance matrix of process noise signifies the covariance among the errors of state elements, which can be examined based on the source of the errors.

This Immediate UKF approach is chosen to provide real-time predictions of the vehicle's state after receiving environmental data. Therefore, the UKF prediction step is employed to forecast the state for the next timestamp. Furthermore, upon receiving environmental data, a validation and update step is conducted on the previous vehicle state prediction before proceeding with the prediction of the state for the next timestamp, with details referring to the flowchart in Algorithm 1. This cyclic process is further detailed in the following two steps.

3) Observation and Validation: In each iteration of the immediate UKF process, this and next step is performed as a top priority. It involves the validation and update of the previous vehicle state prediction using the data received in the current step. For a detailed illustration of this procedure, please refer to the flowchart in Algorithm 1.

Each of the observation (measurement) point is instantiated as follows:

$$Z_i(t) = H[X_i(t)], \quad i = 0, ..., 2L$$
 (14)

Then the observation mean can be obtained as:

$$\hat{z}(t) = \sum_{i=0}^{i=2L} W_i^m Z_i(t)$$
 (15)

The validation region represents a critical threshold that is linked to the acceptability of observation values. It is crucial to emphasize that these values hold validity only when observation values fall within the validation region. Consequently, the validation region can be defined as follows:

$$\Phi_{i}(t, \varepsilon^{2}) = \{v: [Z_{i}(t) - \hat{z}(t)]^{T} \times [P_{zz}^{i}(t|t)]^{-1} \times [Z_{i}(t) - \hat{z}(t)] \le \varepsilon^{2}\}$$
(16)

Where the threshold parameter ε corresponds to the number of sigma points. Additionally, opt for 2n + 1 sigma points, where n represents the dimension of the random variable. Given the additive and independent nature of measurement noise, the innovation covariance matrix is determined in the following equation:

$$P_{zz}(t) = \sum_{i=0}^{i=2L} W_i^c \{ [Z_i(t) - \hat{z}(t)] \times [Z_i(t) - \hat{z}(t)]^T \} + R(t)$$
(17)

where R(t) represents the covariance matrix of the measurement noise at current timestamp.

The source of measuring noise covariance is the temporal and spatial asynchrony error when receiving BSMs message sets.

4) Update: The computation of near-optimal Kalman gain can be calculated as:

$$K(t) = P_{xz}(t|t-1) \times P_{zz}^{-1}(t)$$
(18)

with the cross correlation matrix:

$$P_{xz}(t|t-1) = \sum_{i=0}^{i=2L} W_i^c \{ [X_i(t|t-1) - \hat{x}(t|t-1)] * [Z_i(t) - \hat{z}(t)]^T \}$$
 (19)

The update information about the estimated mean state and the covariance matrix is, respectively:

$$\hat{x}(t|t) = \hat{x}(t|t-1) + K(t) \times (Z(t) - \hat{z}(t))$$

$$P_{yy}(t|t) = P_{yy}(t|t-1) + K(t) \times P_{yy}^{-1}(t) \times K(t)^{T}$$
(20)

IMM algorithm:

Algorithm 2 IMM Algorithm

for $step \ episode = 1$, $Max \ steps \ do$

Interaction:

(1) Calculate the mixing probability $\mu_{ij}(t+1)$

Model matched filtering:

- (1) Calculate the initial state $\tilde{x}_i(t)$
- (2) Calculate the associated mixing error covariance $\tilde{P}_{j}(t)$

Model matched filtering:

(1) The probability update $\mu_i(t+1)$

Combination:

- (1) Calculate the combined state $\hat{x}(t+1)$
- (2) Calculate the associated mixing error covariance P(t+1)

end

Due to the highly nonlinear nature of vehicle dynamics and the continuously changing behavior in complex traffic intersections, the choice of an appropriate motion model combined with the state prediction method is of utmost importance. In pursuit of this objective, an Interactive Multiple Model (IMM) algorithm is implemented, combining the Immediate UKF prediction approach and several motion models to replace the solitary model only.

IMM can be characterized by the transition probabilities of the models at each iteration, offering a dependable solution for predicting motion and occupancy during consistent changes in driving behavior. The IMM algorithm comprises four steps, outlined in Algorithm 2. The linear complexity of the IMM algorithm is evident from the number of iterations specified in the algorithm.

First, we define a set of five Immediate UKF models with different motion control module:

$$M = \{M_{CL}^{UKF}, M_{CV}^{UKF}, M_{CA}^{UKF}, M_{CL}^{UKF}, M_{VT}^{UKF}\}$$
 (21)

each motion model has already been illustrated in the equations of (4)-(8)

Applying the Markov model, the probability of transitioning between states at a particular moment is only relied on its preceding state. It is assumed that for each timestamp, there exists a probability denoted as p_{ij} , signifying a transition from model i to model j, namely:

$$p_{ij} \triangleq p(M_i(t+1)|M_i(t)), \quad i,j \in \{CL,CV,CA,CJ,VT\}$$
 (22)

where $0 < p_{ij} < 1$, and if i is certain, then the sum of p_{ij} over all j ($j \in \{CL, CV, CA, CJ, VT\}$) equals 1.

In the Markov model, given an initial state, subsequent to the transformation of the state transition matrix, the system will ultimately reach a stable state. This involves iteratively computing probability updates until a stable equilibrium state is attained. Assuming a prior of the probability for each model, namely, $\mu_r(0) = p(M_r(0)), r \in \{CL, CV, CA, CJ, VT\}$. The initial value of the probability transition matrix is utilized and subsequently computed iteratively according to Algorithm 2. The linear complexity of the IMM algorithm, as mentioned in previous research, implies that the probability transition matrix will converge to a certain value with minimal fluctuation. The resulting converged value represents the probability transition matrix.

1) Interaction: The IMM procedure initiates with the computation of the mixing probability for the interaction process. The normalized mixing probability $\mu_{ij}(t+1)$, derived from the probability transition matrix and the outcome of the preceding recursive probability $\mu_{ij}(t)$, is determined as follows:

$$\mu_{ij}(t+1) = \frac{1}{c_j} p_{ij} \mu_i(t), \quad i, j \in \{CL, CV, CA, CJ, VT\}$$
 (23)

with

$$\overline{c}_j = \sum_i p_{ij} \mu_i(t)$$

2) Model Matched Filtering: The calculation of the filter input is performed to estimate the initial mixing state $\tilde{x}_j(t)$ and the corresponding mixing error covariance $\tilde{P}_j(t)$ based on the mixing probability

$$\tilde{x}_{j}(t) = \sum_{i} \mu_{ij}(t) \hat{x}_{i}(t), \quad i, j \in \{CL, CV, CA, CJ, VT\}$$

$$\tilde{P}_{j}(t) = \sum_{i} \mu_{ij}(t) \left(P_{i}(t) + \left(\hat{x}_{i}(t) - \tilde{x}_{j}(t) \right) \left(\hat{x}_{i}(t) - \tilde{x}_{j}(t) \right)^{T} \right)$$
(24)

with

$$(\widehat{x}_i(t+1),P_i(t+1)) = \mathcal{F}_i\big(\widetilde{x}_i(t),\widetilde{P}_i(t)\big)$$

where $\mathcal{F}_i(\cdot)$ represents the function of filter output for the model *i*. Meanwhile, $\hat{x}_i(t)$ and $P_i(t)$ are the filter output state and the associated covariance at timestamp *t*, respectively.

3) Model Probability Update: The probability update $\mu_i(t+1)$ for model i at timestamp t+1 can be deduced based on the likelihood function Λ_i as outlined below:

$$\mu_i(t+1) = \frac{1}{c}\Lambda_i(t+1)\overline{c}_i \tag{25}$$

with the normalization constant:

$$c = \sum_{i} \Lambda_i(t+1)\hat{x}_i(t+1) \tag{26}$$

4) Combination: The combined state $\hat{x}(t+1)$ and its covariance $\hat{P}(t+1)$ can be obtained as follow:

$$\hat{x}(t+1) = \sum_{i} \mu_{j}(t+1)\hat{x}_{i}(t+1), \quad i, j \in \{CL, CV, CA, CJ, VT\}$$

$$P(t+1) = \sum_{i} \mu_{i}(t+1) \times \{P_{i}(t+1) + [\hat{x}_{i}(t+1) - \hat{x}(t+1)] \times [\hat{x}_{i}(t+1) - \hat{x}(t+1)]^{T}\}$$
(27)

In summary, relying on V2X data from other vehicles transmitted via BSM, including their positions, velocities, and heading angles, as well as the ego vehicle's own state data, five distinct motion models have been established. The Interactive Multiple Model Unscented Kalman Filter (IMM-UKF) is applied to select and control these models, enabling real-time prediction of the future motion states of the vehicles. Then, the sizes and heading angles of vehicles are applied to establish its occupancy in the predicted BEV map. These form the basis for the fusion prediction of vehicles states encompassing both motion and occupancy.

C. Driving Planning and Control

The driving planning and control is conducted within a self-constructed environment of Deep Reinforcement Learning (DRL). This environment integrates all perceptual information, predictive content, traffic rules, and road events. Subsequently, a reward function is applied, fostering interaction between the ego vehicle and the above elements during training. Neural networks are employed to establish relationships among them. The specific methodology in DRL includes principles of vehicle kinematics and dynamics, the observation of agent, agent action selection, reward functions, and reward shaping approach.

Kinematics Vehicle Model

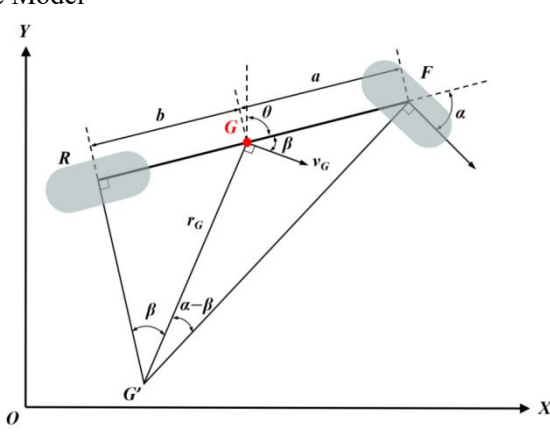


Fig. 2. "Bicycle" model

The "bicycle model" is a kinematic vehicle model illustrated in Figure 2. In this model, the traditional pairs of left and right wheels, both in the front and rear, are abstracted into two virtual wheels positioned in the middle of the vehicle. The steering angle of the front wheel is denoted as α , representing the angular difference between the vehicle's longitudinal axis and the orientation of the front wheel. The vehicle's center of gravity, designated as G, is located at distances a and b from the front and rear wheels, respectively. In the global coordinate frame, (x, y) signifies the coordinates of point G, while v_G represents the velocity vector located at point G. The angle θ denotes the yaw angle at last timestamp, and β characterizes the turn angle of the vehicle. Additionally, the line r_G corresponds to the radius of the vehicle's motion path, and the term $\overline{\theta} = \theta + \beta$ signifies the yaw angle at current timestamp.

By applying the "Sine Rule" to triangle G'GF and G'GR, the following equations can be easily derived:

$$\frac{\sin\left(\frac{\pi}{2} - \alpha\right)}{r_G} = \frac{\sin\left(\alpha - \beta\right)}{a}, \qquad \frac{\sin\left(\frac{\pi}{2}\right)}{r_G} = \frac{\sin\beta}{b}.$$
 (28)

Rearranging (28) leads to

$$\tan \alpha \cos \beta = \frac{a+b}{r_G} \tag{29}$$

Using (28) and (29), the turn angle β of vehicle can be obtained as

$$\beta = \tan^{-1} \left(\frac{b \tan \alpha}{a + b} \right) \tag{30}$$

Therefore, using (30) and the yaw angle at previous timestamp θ , the yaw angle at current timestamp $\bar{\theta}$ can be computed as

$$\bar{\theta} = \theta + \beta = \theta + \tan^{-1}\left(\frac{b\tan\alpha}{a+b}\right) \tag{31}$$

Dynamics Vehicle Model

The dynamics vehicle model would be transformed into a discrete vehicle motion model by employing the Euler implicit method, and the location of G represents the global coordinates of the vehicle (x, y). Specifically, if the action of ego vehicle is remain the state, which means continue the velocity and yaw angle at the last timestamp. The ego vehicle's position (\bar{x}, \bar{y}) , velocity (\bar{v}_x, \bar{v}_y) and yaw angle $\bar{\theta}$ at the current timestamp can be computed as

$$\begin{pmatrix} \overline{x} \\ \overline{y} \\ \overline{v}_{x} \\ \overline{v}_{y} \\ \overline{\theta} \end{pmatrix} = \begin{pmatrix} x + v_{G} \sin \theta \times \Delta T \\ y + v_{G} \cos \theta \times \Delta T \\ v_{G} \sin \theta \\ v_{G} \cos \theta \\ \theta \end{pmatrix}$$
(32)

If the action of ego vehicle is accelerate or decelerate, and the acceleration is a. Then the velocity of ego vehicle at current timestamp \bar{v}_G can be obtain as:

$$\bar{v}_G = v_G + a \times \Delta T \tag{33}$$

Combining (33), the ego vehicle's position (\bar{x}, \bar{y}) , velocity (\bar{v}_x, \bar{v}_y) and yaw angle $\bar{\theta}$ at the current timestamp can be computed as

$$\begin{pmatrix}
\bar{x} \\
\bar{y} \\
\bar{v}_{x} \\
\bar{v}_{y}
\end{pmatrix} = \begin{pmatrix}
x + \bar{v}_{G} \sin \theta \times \Delta T \\
y + \bar{v}_{G} \cos \theta \times \Delta T \\
\bar{v}_{G} \sin \theta \\
\bar{v}_{G} \cos \theta
\end{pmatrix}$$

$$(34)$$

If the action of ego vehicle is turn left or turn right, and the steering angle is α . Then combining (31) in the kinematic vehicle model, the ego vehicle's position (\bar{x}, \bar{y}) , velocity (\bar{v}_x, \bar{v}_y) and yaw angle $\bar{\theta}$ at the current timestamp can be obtained as

$$\begin{pmatrix} \overline{x} \\ \overline{y} \\ \overline{v}_{x} \\ \overline{v}_{y} \end{pmatrix} = \begin{pmatrix} x + v_{G} \sin \overline{\theta} \times \Delta T \\ y + v_{G} \cos \overline{\theta} \times \Delta T \\ v_{G} \sin \overline{\theta} \\ v_{G} \cos \overline{\theta} \\ \theta + tan^{-1} \left(\frac{b \tan \alpha}{a + b} \right) \end{pmatrix}$$
(35)

Observation: This represents the content observed at each step by the agent.

- 1) Relative position of goal (including shaped goals and the final goal)
- 2) Agent velocity
- 3) Agent yaw angle
- 4) Judgment of in-road
- 5) Distance to the lane line
- 6) Distance to the nearest position of off-road
- 7) Relative position to obstacle area
- 8) Relative position to the stop line of traffic signal light
- 9) Traffic signal light phase and countdown
- 10) At most ten other vehicles' driving states (relative position, velocity and yaw angle)
- 11) A current timestamp bird's-eye view gray-scale image with the agent at the center
- 12) A predicted next timestamp bird's-eye view gray-scale image with the agent at the center

Action: These are the actions that the agent can take

- 1) Remain state (velocity and yaw angle)
- 2) Accelerate: acceleration $a = 1 \text{ m/s}^2$
- 3) Decelerate: acceleration $a = -1 \text{ m/s}^2$
- 4) Turn left: steering angle $\alpha = -\pi/6 \, rad$
- 5) Turn right: steering angle $\alpha = \pi/6 \, rad$

Reward Function: This is a weighted sum of the reward components shaped according to ego vehicle states, interactions involving surrounding vehicles, and key traffic events.

```
Rewards + = \begin{cases}
-500 & \text{terminated} & \text{if} : \text{collision with other vehicles} \\
-500 & \text{terminated} & \text{if} : \text{passing stop line during red light} \\
-500 & \text{terminated} & \text{if} : \text{passing stop line during red light} \\
-500 & \text{terminated} & \text{if} : \text{exceeding the } Max\_steps \text{ without reaching final goal} \\
-100 & \text{if} : \text{predicted agent collision or other dangerous events} \\
(200 - step\_episode) * \sqrt{shaped\_num + 1} & \text{if} : \text{arriving at shaped goals (36)} \\
-5 & \text{if} : \text{occupied the lane line} \\
-1000 & \text{if} : \text{terminated} \\
1000 & \text{if} : \text{arriving at the final goal} \\
-(acceleration)^2 * 10 & \text{if} : \text{action is accelerate or decelerate}
\end{cases}
                                                                                                             00 & terminated if: driving in area of off-road, reverse-road and obstacle
```

Reward shaping method:

When applying DQN to address decision-making and driving planning problems in complex traffic environments, there is often a need for certain essential extensions of DRL. These extensions are aimed at enhancing the scalability, learning speed, and overall performance convergence of the algorithm within complicated problem domains.

Reward shaping is a common extension to improve the overall performance convergence of DRL environment and serves as a powerful mechanism for accelerating the learning speed of DRL agents by empirical evidence [80]. In cases where a DRL agent may undergo a long period in discovering the objectives when learning from delayed rewards, the concept of shaping accelerates the learning process by rewarding all behaviors that steer towards the desired actions. Through the method of reward shaping, it becomes possible to design a reward function that imparts more frequent feedback signals concerning suitable behaviors [81], a particularly valuable approach in domains with sparse rewards. In general, the adjustment of the return derived from the reward function is: r' = r + f, where r represents the return from the original reward function R, f stands for the supplementary reward offered by a shaping function F, and F' denotes the signal provided to the agent via the expanded reward function R'.

The Fig. 3. illustrate the reward shaping design, where the yellow block represents the goals associated with the particular reward in reward function (36), including the shaped reward with shaped goals and the ultimate ones.

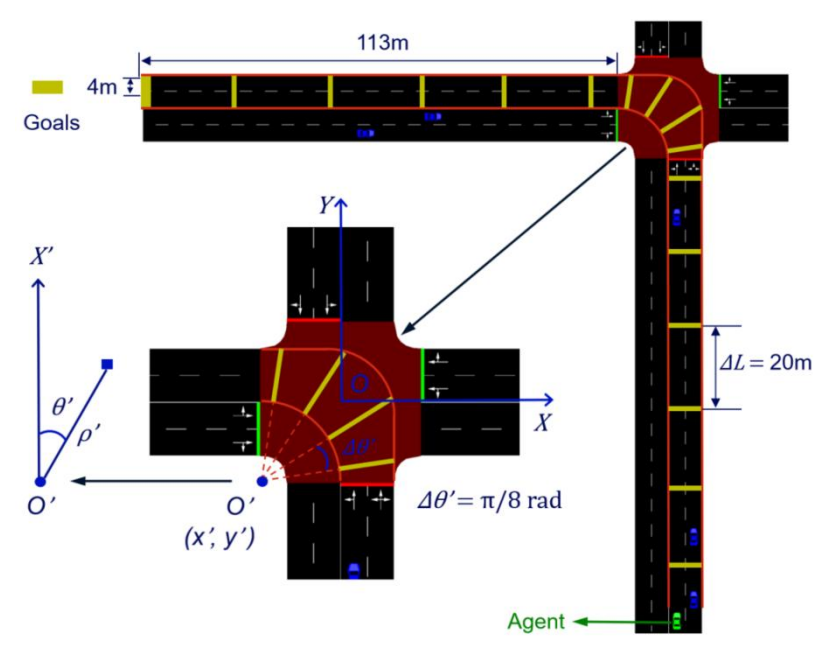


Fig. 3. the design of reward shaping for a DRL agent in traffic intersection

In the straight road, the shaped goals accompanied by shaped reward in (36) are separated and placed at fixed intervals of 20 meters, covering the whole width range of road. However, as the agent need maneuver turning left to arrive at the ultimate goal, the position and covering range

of shaped goals in the intersection area should be expressed by polar coordinates. Then with the presentation of Fig. 3, the Cartesian - polar coordinates transformation in intersection can be computed as follow:

$$x' = x - w, \ y' = y - w$$

$$\rho' = \sqrt{x'^2 + y'^2}$$

$$\theta' = tan^{-1} (x'/y')$$
(37)

where (x, y) is the Cartesian coordinates in BEV presentation, (x', y') is the transformed coordinates for polar presentation, w is the half width of the center intersection area. Then the polar axis is oriented in the direction of a yaw angle of 0, which is the true north direction. And ρ' and θ' is the polar radius and the polar angle, respectively. Where $\theta' \in (0, \pi/2)$, and when turning left, $\theta' : \pi/2 \to 0$.

The covering range of can be divined into three phases according to the polar angle:

1st phase: when $\theta' \epsilon(0, \tan^{-1}(1/2))$, the minimum and maximum of radius can be computed as:

$$\rho'_{min} = w$$

$$\rho'_{max} = 2w/\cos\theta'$$

$$\theta'\epsilon(0, \tan^{-1}(1/2))$$
(38)

with

2nd phase: when $\theta' \epsilon(\tan^{-1}(1/2), \tan^{-1}(2))$, the minimum and maximum of radius can be formulated as:

$$\rho'_{min} = w$$

$$\rho'_{max} = \sqrt{5}w$$

$$\theta' \epsilon (\tan^{-1}(1/2), \tan^{-1}(2))$$
(39)

with

3rd phase: when $\theta' \epsilon(\tan^{-1}(2), \pi/2)$, the minimum and maximum of radius can be calculated as:

$$\rho'_{min} = w$$

$$\rho'_{max} = 2w/\sin\theta'$$
 (40) with
$$\theta' \epsilon(\tan^{-1}(2), \pi/2)$$

In the center intersection area, combining the polar radius and polar angle in the equations (37-40), and the reward function (36), the shaped goals with shaped reward are divided and placed at fixed intervals of polar angle $\pi/8$, as shown in Fig. 3.

IV. TESTING RESULTS

In order to verify the effectiveness and performance of this autonomous driving model with interconnected functions, we conduct a series of simulation experiments. First, the BEV-V2X perception map was constructed. Subsequently, both the motion and occupancy predictions for all vehicles were accomplished. Finally, integrating the preceding works, a model was trained to complete driving decision-making and planning.

A. BEV-V2X Perception

The detailed diagram in Fig. 4 illustrates the establishment of road connectivity using the V2X (MAP) message set. It depicts the process of transforming the information required in the MAP messages from Section III.A into locally coordinated data. This process results in the construction of a global BEV perception map for road connectivity.

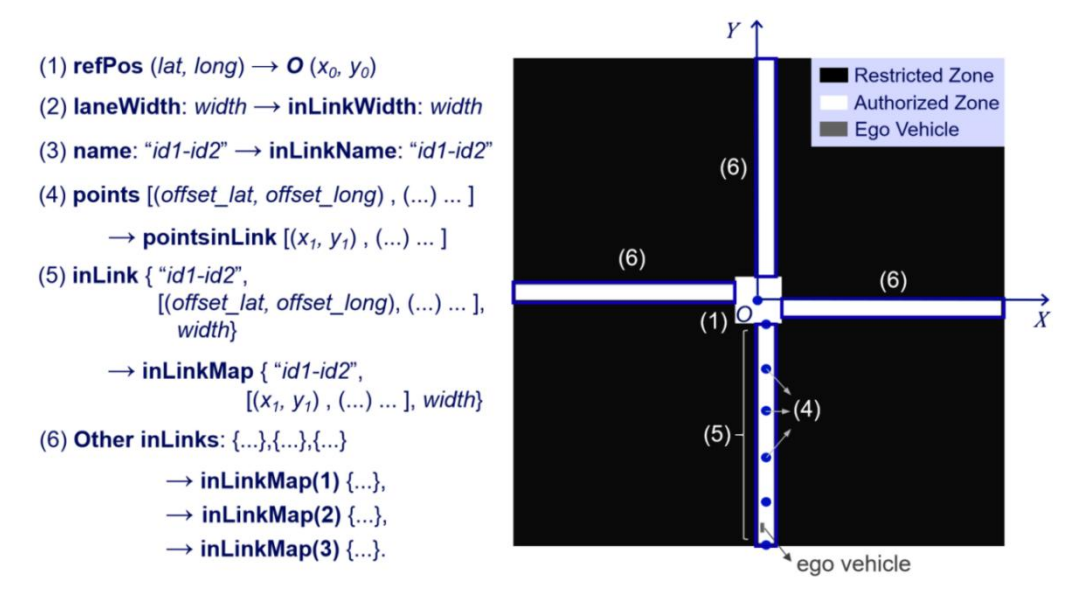


Fig. 4. Details on the construction for road connectivity

Subsequently, the constructed content of Traffic Signal Light Information, Road Event and Traffic Sign Information, and Other Vehicles Information from Section III.A is applied to the BEV local map. This results in a comprehensive map comprising authorized driving areas, occupancy regions by vehicles, dangerous areas, and traffic signal light information (utilizing the stop line to determine passage permission). The global BEV-V2X perception map is illustrated in Fig. 5.

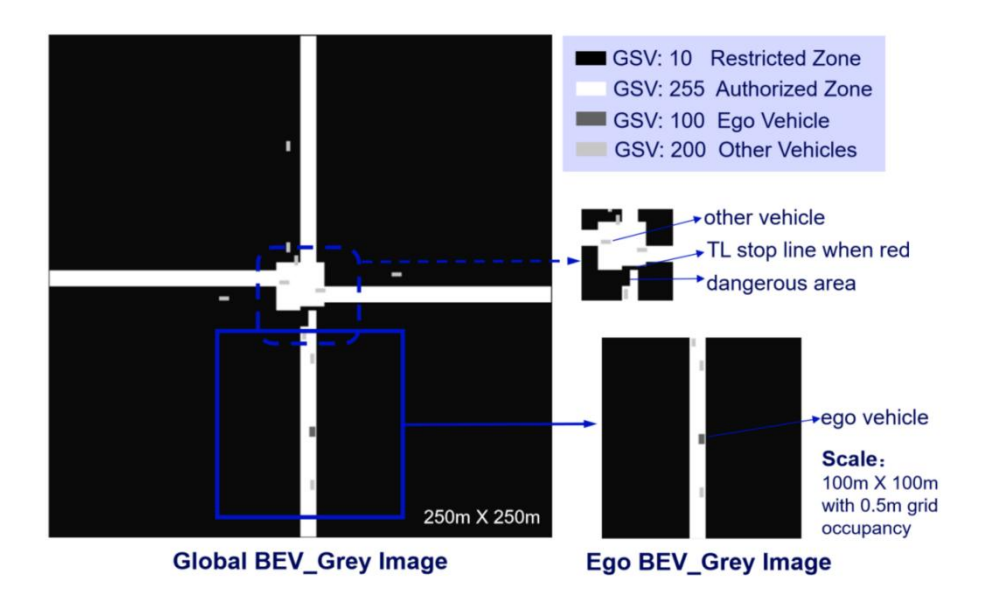


Fig. 5. BEV-V2X perception map

In Fig. 5, the BEV_Grey map utilizes different grayscale values to represent various elements, encompassing distinctive features of agents, other vehicles, and scene information. Subsequently, a local ego BEV_Grey map centered around the ego vehicle is segmented from the global BEV map, serving as the input for perception data into the driving planning module for learning. The primary objective is to eliminate redundant information, accelerate convergence, and improve the training speed.

B. Motion and Occupancy Prediction

Applying the fusion prediction method (IMM-UKF) from Section III.A, the real-time motion and occupancy predictions are conducted for all vehicles. Initially, the state information (position, velocity, heading angle, etc.) for all vehicles is used to predict their states and occupancy within a one-second, determining the vehicle's future state information. This information is then combined with the vehicle sizes to construct occupancy on the BEV Grey map.

As shown in Fig. 6, the real-time motion and occupancy prediction for the left turning of the ego vehicle is depicted. The top row illustrates the actual ego vehicle grayscale map during the left turning process in the intersection. The second row represents the prediction map for all vehicles at each time point. The timestamps in each column of images are equal, with the upper images representing the actual BEV map and the lower images representing the predicted BEV map.

Fact: Time direction Predicted:

Fig. 6. The motion and occupancy prediction for ego vehicle left turning

Fig. 6 illustrates that through prediction, it is possible to proactively perceive the interactions between the ego vehicle and other vehicles or drivable areas. This enables anticipatory operations such as decelerating in advance, adjusting ego posture to avoid collisions, and providing a reference for proactive motions. Similarly, the predicted ego BEV_Grey map centered around the ego vehicle is input into the driving planning module for training. This contributes to providing more valuable predictive information for interactive driving exploration and functionalities.

C. Decision-Making and Driving Planning

The driving decision-making and driving planning module adopts the approach from Section III.C, establishing a Deep Reinforcement Learning (DRL) environment. This involves incorporating perception and prediction information, road rules, and objectives into the reward and penalty functions for training the ego vehicle (agent), in planning and control.

During the inference process, the entire DRL model collaborates with SUMO software to enable the transmission of V2X information and showcase its outcomes. As depicted in Fig. 7, it illustrates the driving planning and control operations of the ego vehicle during the changing-lane phase on a straight road and the left-turning phase within an intersection, along with corresponding timestamps (blue), ego vehicle states (green), and action parameters (red) annotated in the Fig. 7.

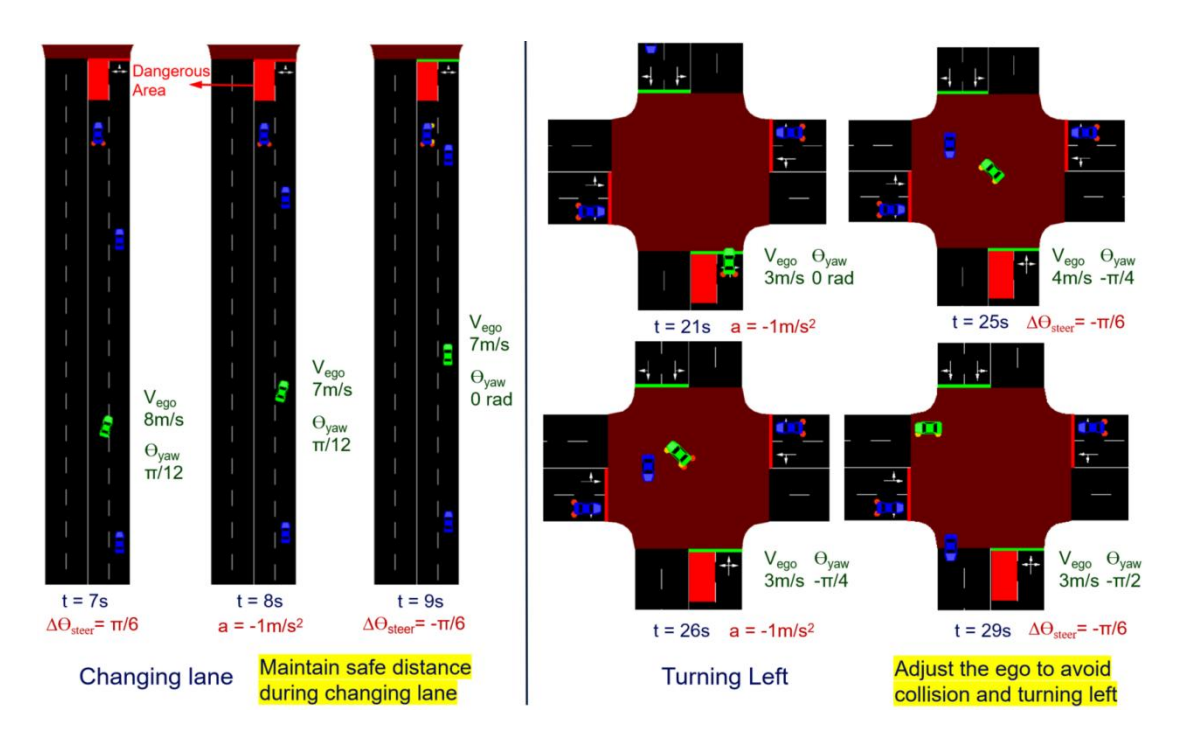


Fig. 7. The changing-lane phase and the left-turning phase of ego vehicle for driving planning results

During the lane-changing phase on the left side of Fig. 7, it can be observed that the ego vehicle, upon anticipating the presence of a non-navigable hazardous area ahead, decides to change lanes for overtaking. Prior to the lane change, it adjusts its speed to maintain a safe distance from fast and slow-moving vehicles in the adjacent lane. While changing lane, it initiates a right turn, subsequently decelerates to ensure safety in posture and motion, and then completes the lane change with a left turn at the same angle. The entire process reflects anticipatory decision-making based on road conditions, showcasing a high level of driving planning safety.

The right side of Fig. 7 illustrates the left-turning phase within the intersection, involving operations such as navigating through a green light, continuous left turning, and making way for oncoming vehicles. Initially, the ego vehicle decelerates during the green light period, smoothly crosses the signal light stop line, and enters the intersection. Subsequently, it engages in continuous left turning by adjusting the overall posture through steering, acceleration, and deceleration. Anticipating and predicting the risk of collision with oncoming vehicles during the left turn, the ego vehicle proactively decelerates to avoid to the vehicles proceeding straight. Finally, it smoothly exits the intersection by consistently adjusting the vehicle's posture, completing the turning left operation. The entire process demonstrates the vehicle's intelligent navigation through driving planning, integrating perception and prediction. The interactive game

planning and safety of the overall operation resemble an experienced human driver, showcasing a high level of driving planning intelligence.

V. FURTHER DISCUSSION

While this solution provides a comprehensive autonomous driving model, there is still much work to be done for improvement, including designing integrated learnable algorithms to enhance the efficiency and generalization, establishing interactive game predictions over long time intervals and testing the model using different datasets to validate its general effectiveness.

VI. CONCLUSIONS

This study presents an autonomous driving model that utilizes V2X-ITS perception data technology to construct a BEV perception map, employs IMM-UKF for motion and occupancy predictions of the ego and nearby vehicles, and establishes a DRL environment to train the agent for decision-making and driving planning. Finally, the model is trained and tested through the same dateset, presenting integrated driving behaviors that encompass obstacle avoidance, overtaking, lane changing, turning maneuver, and synchronized signal light navigation. This work provides a feasible and comprehensive solution for the research and application of connected intelligent vehicles (CAVs) using V2X technology in autonomous driving scenarios.

REFERENCES

- [1] J. Wang, Y. Shao, Y. Ge, and R. Yu, "A Survey of Vehicle to Everything (V2X) Testing.," *Sensors (Basel)*, vol. 19, no. 2, Jan. 2019, doi: 10.3390/s19020334.
- [2] Z. MacHardy, A. Khan, K. Obana, and S. Iwashina, "V2X Access Technologies: Regulation, Research, and Remaining Challenges," *IEEE Commun. Surv. Tutorials*, vol. 20, no. 3, pp. 1858–1877, 2018, doi: 10.1109/COMST.2018.2808444.
- [3] V. Maglogiannis, D. Naudts, S. Hadiwardoyo, D. Van Den Akker, J. Marquez-Barja, and I. Moerman, "Experimental V2X Evaluation for C-V2X and ITS-G5 Technologies in a Real-Life Highway Environment," *IEEE Trans. Netw. Serv. Manage.*, vol. 19, no. 2, pp. 1521–1538, Jun. 2022, doi: 10.1109/TNSM.2021.3129348.
- [4] A. Costandoiu and M. Leba, "Convergence of V2X communication systems and next generation networks," *IOP Conf. Ser.: Mater. Sci. Eng.*, vol. 477, p. 012052, Feb. 2019, doi: 10.1088/1757-899X/477/1/012052.
- [5] M. H. C. Garcia *et al.*, "A Tutorial on 5G NR V2X Communications," *IEEE Commun. Surv. Tutorials*, vol. 23, no. 3, pp. 1972–2026, 2021, doi: 10.1109/COMST.2021.3057017.
- [6] K. Ganesan, P. B. Mallick, J. Lohr, D. Karampatsis, and A. Kunz, "5G V2X Architecture and Radio Aspects," in 2019 IEEE Conference on Standards for

- Communications and Networking (CSCN), Granada, Spain: IEEE, Oct. 2019, pp. 1–6. doi: 10.1109/CSCN.2019.8931319.
- [7] S. Chen *et al.*, "Vehicle-to-Everything (v2x) Services Supported by LTE-Based Systems and 5G," *IEEE Comm. Stand. Mag.*, vol. 1, no. 2, pp. 70–76, 2017, doi: 10.1109/MCOMSTD.2017.1700015.
- [8] K. Sehla, T. M. T. Nguyen, G. Pujolle, and P. B. Velloso, "Resource Allocation Modes in C-V2X: From LTE-V2X to 5G-V2X," *IEEE Internet Things J.*, vol. 9, no. 11, pp. 8291–8314, Jun. 2022, doi: 10.1109/JIOT.2022.3159591.
- [9] A. Alalewi, I. Dayoub, and S. Cherkaoui, "On 5G-V2X Use Cases and Enabling Technologies: A Comprehensive Survey," *IEEE Access*, vol. 9, pp. 107710–107737, 2021, doi: 10.1109/ACCESS.2021.3100472.
- [10] R. Molina-Masegosa and J. Gozalvez, "LTE-V for Sidelink 5G V2X Vehicular Communications: A New 5G Technology for Short-Range Vehicle-to-Everything Communications," *IEEE Veh. Technol. Mag.*, vol. 12, no. 4, pp. 30–39, Dec. 2017, doi: 10.1109/MVT.2017.2752798.
- [11] K. C. Dey, A. Rayamajhi, M. Chowdhury, P. Bhavsar, and J. Martin, "Vehicle-to-vehicle (V2V) and vehicle-to-infrastructure (V2I) communication in a heterogeneous wireless network Performance evaluation," *Transportation Research Part C: Emerging Technologies*, vol. 68, pp. 168–184, Jul. 2016, doi: 10.1016/j.trc.2016.03.008.
- [12] M. Kutila, K. Kauvo, Y. Zheng, X. Zhang, and V. Garrido Martinez, "EU-China Joint V2X Trial Results," in *Proceedings of the 2021 Joint European Conference on Networks and Communications & 6G Summit (EuCNC/6G Summit)*, 2021. [Online]. Available: https://www.eucnc.eu/
- [13] Z. Lei, S. Ren, Y. Hu, W. Zhang, and S. Chen, "Latency-Aware Collaborative Perception," in *Computer Vision ECCV 2022*, S. Avidan, G. Brostow, M. Cissé, G. M. Farinella, and T. Hassner, Eds., Cham: Springer Nature Switzerland, 2022, pp. 316–332.
- [14] S. Wei *et al.*, "Asynchrony-Robust Collaborative Perception via Bird's Eye View Flow," in *Thirty-seventh Conference on Neural Information Processing Systems*, 2023. [Online]. Available: https://openreview.net/forum?id=UHIDdtxmVS
- [15] H. Yu, Y. Tang, E. Xie, J. Mao, P. Luo, and Z. Nie, "Flow-Based Feature Fusion for Vehicle-Infrastructure Cooperative 3D Object Detection," 2023, doi: 10.48550/ARXIV.2311.01682.
- [16] H. Yu et al., "DAIR-V2X: A Large-Scale Dataset for Vehicle-Infrastructure Cooperative 3D Object Detection," in *Proceedings of the IEEE/CVF Conference on Computer Vision and Pattern Recognition (CVPR)*, Jun. 2022, pp. 21361–21370.
- [17] S. Fan, H. Yu, W. Yang, J. Yuan, and Z. Nie, "QUEST: Query Stream for Practical Cooperative Perception," 2023, doi: 10.48550/ARXIV.2308.01804.
- [18] H. Yu et al., "V2X-Seq: A Large-Scale Sequential Dataset for Vehicle-Infrastructure Cooperative Perception and Forecasting," in *Proceedings of the IEEE/CVF Conference on Computer Vision and Pattern Recognition (CVPR)*, Jun. 2023, pp. 5486–5495.
- [19] E. Guo, Z. Chen, S. Rahardja, and J. Yang, "3D Detection and Pose Estimation of Vehicle in Cooperative Vehicle Infrastructure System," *IEEE Sensors J.*, vol. 21, no. 19, pp. 21759–21771, Oct. 2021, doi: 10.1109/JSEN.2021.3101497.

- [20] Y. Hu, S. Fang, Z. Lei, Y. Zhong, and S. Chen, "Where2comm: Communication-Efficient Collaborative Perception via Spatial Confidence Maps," in *Advances in Neural Information Processing Systems*, S. Koyejo, S. Mohamed, A. Agarwal, D. Belgrave, K. Cho, and A. Oh, Eds., Curran Associates, Inc., 2022, pp. 4874–4886. [Online]. Available:
- https://proceedings.neurips.cc/paper_files/paper/2022/file/1f5c5cd01b864d53cc5fa0a3472e15 2e-Paper-Conference.pdf
- [21] R. Xu, H. Xiang, Z. Tu, X. Xia, M.-H. Yang, and J. Ma, "V2X-ViT: Vehicle-to-Everything Cooperative Perception with Vision Transformer," in *Computer Vision ECCV 2022*, vol. 13699, S. Avidan, G. Brostow, M. Cissé, G. M. Farinella, and T. Hassner, Eds., in Lecture Notes in Computer Science, vol. 13699., Cham: Springer Nature Switzerland, 2022, pp. 107–124. doi: 10.1007/978-3-031-19842-7 7.
- [22] C. Chang *et al.*, "BEV-V2X: Cooperative Birds-Eye-View Fusion and Grid Occupancy Prediction via V2X-Based Data Sharing," *IEEE Trans. Intell. Veh.*, vol. 8, no. 11, pp. 4498–4514, Nov. 2023, doi: 10.1109/TIV.2023.3293954.
- [23] "T/CSAE 53-2020. Cooperative intelligent transportation system: vehicular communication; application layer specification and data exchange standard Phase II." Chinese Society of Automotive Engineering, Beijing, 2020.
- [24] G. Ros, S. Ramos, M. Granados, A. Bakhtiary, D. Vazquez, and A. M. Lopez, "Vision-Based Offline-Online Perception Paradigm for Autonomous Driving," in *2015 IEEE Winter Conference on Applications of Computer Vision*, Waikoloa, HI, USA: IEEE, Jan. 2015, pp. 231–238. doi: 10.1109/WACV.2015.38.
- [25] J. Florback, L. Tornberg, and N. Mohammadiha, "Offline object matching and evaluation process for verification of autonomous driving," in 2016 IEEE 19th International Conference on Intelligent Transportation Systems (ITSC), Rio de Janeiro, Brazil: IEEE, Nov. 2016, pp. 107–112. doi: 10.1109/ITSC.2016.7795539.
- [26] S. Chen, J. Shang, S. Zhang, and N. Zheng, "Cognitive map-based model: Toward a developmental framework for self-driving cars," in *2017 IEEE 20th International Conference on Intelligent Transportation Systems (ITSC)*, Yokohama: IEEE, Oct. 2017, pp. 1–8. doi: 10.1109/ITSC.2017.8317627.
- [27] S. Chen, Y. Chen, S. Zhang, and N. Zheng, "A Novel Integrated Simulation and Testing Platform for Self-Driving Cars With Hardware in the Loop," *IEEE Trans. Intell. Veh.*, vol. 4, no. 3, pp. 425–436, Sep. 2019, doi: 10.1109/TIV.2019.2919470.
- [28] B. R. Kiran *et al.*, "Deep Reinforcement Learning for Autonomous Driving: A Survey," *IEEE Trans. Intell. Transport. Syst.*, vol. 23, no. 6, pp. 4909–4926, Jun. 2022, doi: 10.1109/TITS.2021.3054625.
- [29] Z. Li *et al.*, "BEVFormer: Learning Bird's-Eye-View Representation from Multi-camera Images via Spatiotemporal Transformers," in *Computer Vision ECCV 2022*, vol. 13669, S. Avidan, G. Brostow, M. Cissé, G. M. Farinella, and T. Hassner, Eds., in Lecture Notes in Computer Science, vol. 13669. , Cham: Springer Nature Switzerland, 2022, pp. 1–18. doi: 10.1007/978-3-031-20077-9_1.
- [30] T. Roddick and R. Cipolla, "Predicting Semantic Map Representations From Images Using Pyramid Occupancy Networks," in *Proceedings of the IEEE/CVF Conference on Computer Vision and Pattern Recognition (CVPR)*, Jun. 2020.

- [31] C. Chang *et al.*, "MetaScenario: A Framework for Driving Scenario Data Description, Storage and Indexing," *IEEE Trans. Intell. Veh.*, vol. 8, no. 2, pp. 1156–1175, Feb. 2023, doi: 10.1109/TIV.2022.3215503.
- [32] L. Fang, Q. Jiang, J. Shi, and B. Zhou, "TPNet: Trajectory Proposal Network for Motion Prediction," 2020, doi: 10.48550/ARXIV.2004.12255.
- [33] V. Lefkopoulos, M. Menner, A. Domahidi, and M. N. Zeilinger, "Interaction-Aware Motion Prediction for Autonomous Driving: A Multiple Model Kalman Filtering Scheme," *IEEE Robot. Autom. Lett.*, vol. 6, no. 1, pp. 80–87, Jan. 2021, doi: 10.1109/LRA.2020.3032079.
- [34] Y. Guo, D. Yao, B. Li, H. Gao, and L. Li, "Down-Sized Initialization for Optimization-Based Unstructured Trajectory Planning by Only Optimizing Critical Variables," *IEEE Transactions on Intelligent Vehicles*, vol. 8, no. 1, pp. 709–720, 2023, doi: 10.1109/TIV.2022.3163335.
- [35] Y. Hu *et al.*, "Planning-oriented Autonomous Driving," 2022, doi: 10.48550/ARXIV.2212.10156.
- [36] T. P. Lillicrap *et al.*, "Continuous control with deep reinforcement learning," 2015, doi: 10.48550/ARXIV.1509.02971.
- [37] H. Porav and P. Newman, "Imminent Collision Mitigation with Reinforcement Learning and Vision," in 2018 21st International Conference on Intelligent Transportation Systems (ITSC), Maui, HI: IEEE, Nov. 2018, pp. 958–964. doi: 10.1109/ITSC.2018.8569222.
- [38] T. Wang *et al.*, "DeepAccident: A Motion and Accident Prediction Benchmark for V2X Autonomous Driving," 2023, doi: 10.48550/ARXIV.2304.01168.
- [39] Y. Li *et al.*, "V2X-Sim: Multi-Agent Collaborative Perception Dataset and Benchmark for Autonomous Driving," *IEEE Robot. Autom. Lett.*, vol. 7, no. 4, pp. 10914–10921, Oct. 2022, doi: 10.1109/LRA.2022.3192802.
- [40] Y. Huang, J. Du, Z. Yang, Z. Zhou, L. Zhang, and H. Chen, "A Survey on Trajectory-Prediction Methods for Autonomous Driving," *IEEE Trans. Intell. Veh.*, vol. 7, no. 3, pp. 652–674, Sep. 2022, doi: 10.1109/TIV.2022.3167103.
- [41] F. Leon and M. Gavrilescu, "A Review of Tracking and Trajectory Prediction Methods for Autonomous Driving," *Mathematics*, vol. 9, no. 6, p. 660, Mar. 2021, doi: 10.3390/math9060660.
- [42] J. Liu, X. Mao, Y. Fang, D. Zhu, and M. Q.-H. Meng, "A Survey on Deep-Learning Approaches for Vehicle Trajectory Prediction in Autonomous Driving," in *2021 IEEE International Conference on Robotics and Biomimetics (ROBIO)*, Sanya, China: IEEE, Dec. 2021, pp. 978–985. doi: 10.1109/ROBIO54168.2021.9739407.
- [43] S. Mozaffari, O. Y. Al-Jarrah, M. Dianati, P. Jennings, and A. Mouzakitis, "Deep Learning-Based Vehicle Behavior Prediction for Autonomous Driving Applications: A Review," *IEEE Trans. Intell. Transport. Syst.*, vol. 23, no. 1, pp. 33–47, Jan. 2022, doi: 10.1109/TITS.2020.3012034.
- [44] J. Kim *et al.*, "StopNet: Scalable Trajectory and Occupancy Prediction for Urban Autonomous Driving," in *2022 International Conference on Robotics and Automation (ICRA)*, Philadelphia, PA, USA: IEEE, May 2022, pp. 8957–8963. doi: 10.1109/ICRA46639.2022.9811830.
 - [45] Y. Zhang et al., "BEVerse: Unified Perception and Prediction in Birds-Eye-View

- for Vision-Centric Autonomous Driving." arXiv, May 19, 2022. Accessed: Dec. 19, 2023. [Online]. Available: http://arxiv.org/abs/2205.09743
- [46] B. Paden, M. Čáp, S. Z. Yong, D. Yershov, and E. Frazzoli, "A Survey of Motion Planning and Control Techniques for Self-Driving Urban Vehicles," *IEEE Transactions on Intelligent Vehicles*, vol. 1, no. 1, pp. 33–55, 2016, doi: 10.1109/TIV.2016.2578706.
- [47] S. Lefèvre, D. Vasquez, and C. Laugier, "A survey on motion prediction and risk assessment for intelligent vehicles," *Robomech J*, vol. 1, no. 1, p. 1, Dec. 2014, doi: 10.1186/s40648-014-0001-z.
- [48] C. Barrios and Y. Motai, "Improving Estimation of Vehicle's Trajectory Using the Latest Global Positioning System With Kalman Filtering," *IEEE Trans. Instrum. Meas.*, vol. 60, no. 12, pp. 3747–3755, Dec. 2011, doi: 10.1109/TIM.2011.2147670.
- [49] S. Ammoun and F. Nashashibi, "Real time trajectory prediction for collision risk estimation between vehicles," in 2009 IEEE 5th International Conference on Intelligent Computer Communication and Processing, Cluj-Napoca, Romania: IEEE, Aug. 2009, pp. 417–422. doi: 10.1109/ICCP.2009.5284727.
- [50] T. Batz, K. Watson, and J. Beyerer, "Recognition of dangerous situations within a cooperative group of vehicles," in *2009 IEEE Intelligent Vehicles Symposium*, Xi'an, China: IEEE, Jun. 2009, pp. 907–912. doi: 10.1109/IVS.2009.5164400.
- [51] R. E. Kalman, "A New Approach to Linear Filtering and Prediction Problems," *Journal of Basic Engineering*, vol. 82, no. 1, pp. 35–45, Mar. 1960, doi: 10.1115/1.3662552.
- [52] K. Jiang, A. C. Victorino, and A. Charara, "Real-time estimation of vehicle's lateral dynamics at inclined road employing extended Kalman filter," in *2016 IEEE 11th Conference on Industrial Electronics and Applications (ICIEA)*, Hefei, China: IEEE, Jun. 2016, pp. 2360–2365. doi: 10.1109/ICIEA.2016.7603987.
- [53] A. Katriniok and D. Abel, "Adaptive EKF-Based Vehicle State Estimation With Online Assessment of Local Observability," *IEEE Trans. Contr. Syst. Technol.*, vol. 24, no. 4, pp. 1368–1381, Jul. 2016, doi: 10.1109/TCST.2015.2488597.
- [54] T. Lefebvre *, H. Bruyninckx, and J. De Schutter, "Kalman filters for non-linear systems: a comparison of performance," *International Journal of Control*, vol. 77, no. 7, pp. 639–653, May 2004, doi: 10.1080/00207170410001704998.
- [55] E. A. Wan and R. Van Der Merwe, "The unscented Kalman filter for nonlinear estimation," in *Proceedings of the IEEE 2000 Adaptive Systems for Signal Processing, Communications, and Control Symposium (Cat. No.00EX373)*, Lake Louise, Alta., Canada: IEEE, 2000, pp. 153–158. doi: 10.1109/ASSPCC.2000.882463.
- [56] H. Wu, W. Xu, B. Yao, Y. Hu, and H. Feng, "Interacting Multiple Model-Based Adaptive Trajectory Prediction for Anticipative Human Following of Mobile Industrial Robot," *Procedia Computer Science*, vol. 176, pp. 3692–3701, 2020, doi: 10.1016/j.procs.2020.09.330.
- [57] H. Gao, Y. Qin, C. Hu, Y. Liu, and K. Li, "An Interacting Multiple Model for Trajectory Prediction of Intelligent Vehicles in Typical Road Traffic Scenario," *IEEE Trans. Neural Netw. Learning Syst.*, vol. 34, no. 9, pp. 6468–6479, Sep. 2023, doi: 10.1109/TNNLS.2021.3136866.
- [58] J. Quehl, H. Hu, S. Wirges, and M. Lauer, "An Approach to Vehicle Trajectory Prediction Using Automatically Generated Traffic Maps," in 2018 IEEE Intelligent Vehicles

- Symposium (IV), Changshu: IEEE, Jun. 2018, pp. 544–549. doi: 10.1109/IVS.2018.8500535.
- [59] Y. Hu, W. Zhan, and M. Tomizuka, "Probabilistic Prediction of Vehicle Semantic Intention and Motion," in *2018 IEEE Intelligent Vehicles Symposium (IV)*, Changshu: IEEE, Jun. 2018, pp. 307–313. doi: 10.1109/IVS.2018.8500419.
- [60] D. Jeong, M. Baek, and S.-S. Lee, "Long-term prediction of vehicle trajectory based on a deep neural network," in 2017 International Conference on Information and Communication Technology Convergence (ICTC), Jeju: IEEE, Oct. 2017, pp. 725–727. doi: 10.1109/ICTC.2017.8190764.
- [61] W. D. Blair, "Design of nearly constant velocity filters for radar tracking of maneuvering targets," in *2012 IEEE Radar Conference*, Atlanta, GA: IEEE, May 2012, pp. 1008–1013. doi: 10.1109/RADAR.2012.6212285.
- [62] K. Zhang, W. Jiao, L. Wang, Z. Li, J. Li, and K. Zhou, "Smart-RTK: Multi-GNSS kinematic positioning approach on android smart devices with Doppler-smoothed-code filter and constant acceleration model," *Advances in Space Research*, vol. 64, no. 9, pp. 1662–1674, Nov. 2019, doi: 10.1016/j.asr.2019.07.043.
- [63] M. Deng, S. Li, X. Jiang, and X. Li, "Vehicle Trajectory Prediction Method Based on 'Current' Statistical Model and Cubature Kalman Filter," *Electronics*, vol. 12, no. 11, p. 2464, May 2023, doi: 10.3390/electronics12112464.
- [64] M. T. Abbas, M. A. Jibran, M. Afaq, and W. Song, "An adaptive approach to vehicle trajectory prediction using multimodel Kalman filter," *Trans Emerging Tel Tech*, vol. 31, no. 5, p. e3734, May 2020, doi: 10.1002/ett.3734.
- [65] K. Jo, K. Chu, and M. Sunwoo, "Interacting Multiple Model Filter-Based Sensor Fusion of GPS With In-Vehicle Sensors for Real-Time Vehicle Positioning," *IEEE Trans. Intell. Transport. Syst.*, vol. 13, no. 1, pp. 329–343, Mar. 2012, doi: 10.1109/TITS.2011.2171033.
- [66] W. Schwarting, J. Alonso-Mora, and D. Rus, "Planning and Decision-Making for Autonomous Vehicles," *Annu. Rev. Control Robot. Auton. Syst.*, vol. 1, no. 1, pp. 187–210, May 2018, doi: 10.1146/annurev-control-060117-105157.
- [67] Z. Wang *et al.*, "Sample Efficient Actor-Critic with Experience Replay." arXiv, Jul. 10, 2017. Accessed: Dec. 15, 2023. [Online]. Available: http://arxiv.org/abs/1611.01224
- [68] A. M. Devraj and S. P. Meyn, "Fastest Convergence for Q-learning," 2017, doi: 10.48550/ARXIV.1707.03770.
- [69] V. Mnih *et al.*, "Human-level control through deep reinforcement learning," *Nature*, vol. 518, no. 7540, pp. 529–533, Feb. 2015, doi: 10.1038/nature14236.
- [70] M. Zhou, Y. Yu, and X. Qu, "Development of an Efficient Driving Strategy for Connected and Automated Vehicles at Signalized Intersections: A Reinforcement Learning Approach," *IEEE Trans. Intell. Transport. Syst.*, vol. 21, no. 1, pp. 433–443, Jan. 2020, doi: 10.1109/TITS.2019.2942014.
- [71] Y. Guan *et al.*, "Learn collision-free self-driving skills at urban intersections with model-based reinforcement learning," in *2021 IEEE International Intelligent Transportation Systems Conference (ITSC)*, Indianapolis, IN, USA: IEEE, Sep. 2021, pp. 3462–3469. doi: 10.1109/ITSC48978.2021.9564880.
- [72] Y. Shi, Y. Liu, Y. Qi, and Q. Han, "A Control Method with Reinforcement Learning for Urban Un-Signalized Intersection in Hybrid Traffic Environment," *Sensors*, vol. 22, no. 3,

- p. 779, Jan. 2022, doi: 10.3390/s22030779.
- [73] R. Gutiérrez-Moreno, R. Barea, E. López-Guillén, J. Araluce, and L. M. Bergasa, "Reinforcement Learning-Based Autonomous Driving at Intersections in CARLA Simulator," *Sensors*, vol. 22, no. 21, p. 8373, Nov. 2022, doi: 10.3390/s22218373.
- [74] D. Isele, R. Rahimi, A. Cosgun, K. Subramanian, and K. Fujimura, "Navigating Occluded Intersections with Autonomous Vehicles Using Deep Reinforcement Learning," in 2018 IEEE International Conference on Robotics and Automation (ICRA), Brisbane, QLD: IEEE, May 2018, pp. 2034–2039. doi: 10.1109/ICRA.2018.8461233.
- [75] G. Li *et al.*, "Deep Reinforcement Learning Enabled Decision-Making for Autonomous Driving at Intersections," *Automot. Innov.*, vol. 3, no. 4, pp. 374–385, Dec. 2020, doi: 10.1007/s42154-020-00113-1.
- [76] H. Shu, T. Liu, X. Mu, and D. Cao, "Driving Tasks Transfer Using Deep Reinforcement Learning for Decision-Making of Autonomous Vehicles in Unsignalized Intersection," *IEEE Trans. Veh. Technol.*, vol. 71, no. 1, pp. 41–52, Jan. 2022, doi: 10.1109/TVT.2021.3121985.
- [77] D. Kamran, C. F. Lopez, M. Lauer, and C. Stiller, "Risk-Aware High-level Decisions for Automated Driving at Occluded Intersections with Reinforcement Learning," in 2020 IEEE Intelligent Vehicles Symposium (IV), Las Vegas, NV, USA: IEEE, Oct. 2020, pp. 1205–1212. doi: 10.1109/IV47402.2020.9304606.
- [78] T. Tram, I. Batkovic, M. Ali, and J. Sjoberg, "Learning When to Drive in Intersections by Combining Reinforcement Learning and Model Predictive Control," in *2019 IEEE Intelligent Transportation Systems Conference (ITSC)*, Auckland, New Zealand: IEEE, Oct. 2019, pp. 3263–3268. doi: 10.1109/ITSC.2019.8916922.
- [79] M. Hausknecht and P. Stone, "Deep Recurrent Q-Learning for Partially Observable MDPs".
- [80] J. Randløv and P. Alstrøm, "Learning to Drive a Bicycle using Reinforcement Learning and Shaping".
- [81] A. D. Laud, *Theory and application of reward shaping in reinforcement learning*. University of Illinois at Urbana-Champaign, 2004.